A case study of the manufacture of an OTEC factory on a floating ship has been carried out using 100 MW Titanium material at a fairly expensive cost, so the OTEC system was researched using a copper-tin alloy. The behavior of the tin-copper heat exchanger between the Aspen Plus simulation and the Computational Fluid Dynamics (CFD) simulation on Shell And Tube evaporators of Bonnet Divided Flow fixed and Bonnet One-pass Shell fixed (BEM) types is investigated. The difference in temperature between water at sea level of 29 °C and water at a depth of 1000 meters at a temperature of 5 °C is assumed to produce electricity. A marine thermal energy conversion power plant is a continuous source of energy sourced from nature an evaporator heat exchanger with ammonia working fluid will produce power that can drive a turbine forwarded to a generator. The simulation results of CFD of a Bonnet Divided Flow fixed type Heat Exchanger on the hot water inlet line has a temperature of 29.9 °C, when exiting the evaporator shell the temperature decreases to 26.4 °C. At the inlet line, the working fluid of ammonia enters the evaporator at 7.9 °C and when it leaves the tube, the temperature rises to 26.3 °C. The best results of the simulation of Aspen Plus Heat Exchanger type BEM Inlet Ammonia temperature 8 °C and at CFD 7.99 °C. Meanwhile, at the ammonia outlet at 28 °C and in the CFD simulation, the ammonia outlet temperature was 28.21 °C. Aspen Plus Inlet heating water temperature is 30 °C, and in CFD simulation, the temperature is 29.99 °C. While the heating water outlet is 28 °C, and in the CFD simulation, the heating water outlet is 28.15 °C. The conclusion from the simulation results is that the BEM-type heat exchanger is very good and suitable for experimental prototyping

Keywords: OTEC, ORC, renewable energy, CFD simulation, Shell and Tube heat exchanger, seawater temperature, close cycle, copper-tin alloy

UDC 621
DOI: 10.15587/1729-4061.2022.263263

DEVELOPMENT OF TIN COPPER ALLOYS IN SHELL AND TUBE EVAPORATOR HEAT EXCHANGER SYSTEMS IN OCEAN THERMAL ENERGY CONVERSE POWER PLANT

Mawardi
Corresponding author
Doctor's Student in Mechanical Engineering*
Departement of Mechanical Engineering
Universitas Al-Azhar
Jl. Pintu Air IV, 214, Kwala Bekala-Padang Bulan,
Medan, Indonesia, 20142
E-mail: mawardi.ipc@gmail.com
Basuki Wirjosentono
Doctor of Mathematics and Natural Sciences, Professor
Department of Chemistry*
Himsar Ambarita
Doctor of Mechanical Engineering, Professor
Department of Mechanical Engineering*
Jaswar Koto
Doctor of Ocean and Aerospace, Professor,
Vice-Rector for Academic Affair, Research & Development,
and Digital Advancement
Universitas Insan Cita Indonesia
Jl. H. R. Rasuna Said No.Kav. C-18, RT.2/RW.5,
Karet Kuningan, Kecamatan Setiabudi, Kota Jakarta Selatan,
Daerah Khusus Ibukota Jakarta, Indonesia, 12940
*Universitas Sumatera Utara
Jl. Dr. T. Mansur, 9, Kampus Padang Bulan,
Medan, Sumatera Utara, Indonesia, 20155

Received date 12.08.2022
Accepted date 18.10.2022
Published date 31.10.2022

How to Cite: *Mawardi, M., Wirjosentono, B., Ambarita, H., Koto, J. (2022). Development of tin copper alloys in shell and tube evaporator heat exchanger systems in ocean thermal energy converse power plant. Eastern-European Journal of Enterprise Technologies, 5 (8 (119)), 37–52. doi: https://doi.org/10.15587/1729-4061.2022.263263*

1. Introduction

Indonesia is one of the countries with calm sea water and high temperature [1]. Sea surface water temperature can fluctuate annually between 26–30 °C throughout the year [2]. As an archipelagic country located in a subtropical area with a wider sea area than the mainland, Indonesia has the opportunity to produce renewable energy from the sea [3]. Currently, Indonesia needs a large supply of electrical energy because the existing supply is not sufficient for the people's needs. One of the renewable energies that are still little used by the world community, especially in Indonesia, is electrical energy produced from the sea [4]. The difference in seawater temperature at the surface and the bottom can be used to build a power plant called Ocean Thermal Energy Converse (OTEC) [5]. Renewable energy sources that can be extracted using temperature differences from the surface to various depths of air as a source of heat engine propulsion are marine thermal energy conversion systems [6]. OTEC is a renewable energy that is free of harmful emissions and produces stable electrical energy as long as seawater is still on the earth's surface [7]. One of the working principles of OTEC is a that utilizes the seawater temperature at the surface at 29 °C and the sea depth at 5 °C through an evaporator heat

exchanger [8]. This OTEC requires a reliable heat transfer area because the heat exchanger operates in a harsh chemical environment, so a suitable heat exchanger is needed [9]. Previous research on the OTEC closed cycle using a heat exchanger with aluminum and nickel is more economical but short-lived, successful research has been carried out using a heat exchanger with titanium material [10]. The high cost of titanium heat exchangers causes less interest in using OTEC. In addition, titanium replacement material is expected to replace the turbine rotating function [11]. Reengineering technology from the simulation results is carried out directly in the form of prototype objects and test equipment [12]. Based on research on the characteristics of 100 kW OTEC at sea, using ammonia as a working fluid designed a CFD simulation analysis [13].

Therefore, a study devoted to comparing the results of the Aspen Plus simulation with the ANSYS CFD simulation is a study of scientific relevance in modern times. This can contribute to the formation of the design of tool design in the electrical energy distribution network.

2. Literature review and problem statement

This paper [14] aims to create a simulation model using Aspen Plus to determine the effect of parameters such as differences in seawater temperature on the surface and on the seabed. The results showed that the exergy efficiency of the system that directly utilizes ocean thermal energy for desalination reached 7.81 %. The problem is that there is exergy losses, overall energy consumption should also be considered [4]. Simulation studies using Aspen Plus carried out theoretical models and optimization of the marine thermal energy conversion system (OTEC) combined with an organic Rankine generator cycle (ORC) of 125 kW fixed power with 11 working fluids ammonia, R152a, 13R1234yf, R1234ze, R125, R134a, R161, propane, isobutene, RE143a, and perfluorobutane. the result is that for a sea surface temperature of 30 °C and a depth of 5 °C, the net electric power achieved is 94.6 kW for R1234yf, 99.3 kW for ammonia, and 98.0 kW. Only comparing 11 working fluids. The heat exchanger model has not yet been made, so it is necessary to make an OTEC description of the heat exchanger system. Of the 11 simulated working fluids, R1234yf obtains maximum thermodynamics and net electrical efficiency of 3.60 % and ammonia 2.57 %. This article [15] combined OTEC system (Kalina) uses Ammonia-water and isobutane working fluids using aspen plus simulation. The results show that when the turbine inlet pressure exceeds 2.9 MPa and the turbine outlet pressure is between 1.3 and 1.6 MPa in the test range, the proposed cycle is better than the stand-alone system from an energy-saving perspective. But the thing that has not been solved is the low power output. From an energy-efficient perspective, this system is superior, but from the use of fluids, it may need to be considered because of the cost factor [16]. The working fluid and working conditions for the heat exchangers are necessary for an energy efficient and techno-economically feasible OTEC power plant. The following parameters: pipe length, pipe diameter, seawater depth and the flow rate of seawater were considered. The theoretical investigations revealed that a maximum output of the network exists at a certain flow rate of cooling. Heat exchangers are the main component of an OTEC power plant and they play an important role in the economy of an OTEC power plant, hence proper selection of materials, design criteria, working fluid and working conditions for the heat exchanger is necessary for an energy efficient and technologically feasible OTEC power plant. The research methodology [14] uses data collection, digitization, and interpolation. Data is processed using Surfer® software. In this way, a digital terrain model (DTM) map is generated for each sector. The goal is to find the minimum distance to reach a depth of 1000 m as this is the distance at which a temperature difference of 20 °C is obtained. To design a good heat exchanger, with ammonia working fluid, simulations were carried out using Aspen Plus and CFD simulations to compare the results obtained by each model. [17] In this study a new tri-generation system based on OTEC that produces ammonia, cooling, and power was developed and analyzed. An ocean thermal energy conversion-based system are suitable for district cooling, ammonia, and power.

It is therefore prudent and possible to conduct a study comparing the simulation results of Aspen Plus with simulations of ANSYS CFD on shell and tube tin-copper alloy heat exchangers.

3. The aim and objectives of the study

This study aims to compare the results of the Aspen Plus simulation with the ANSYS CFD simulation on a tin-copper alloy heat exchanger shell and tube. To achieve this goal, the following objectives should be achieved:

– design two types of heat exchangers with BJM and BEM types;

– vary the input parameters of the OTEC closed cycle to get the points of variation in the OTEC cycle;

– simulate the inlet and outlet temperatures of the working fluid ammonia and seawater.

4. Materials and methods of the study

Aspen Plus to help design, to operate properly the first steps must be carried out throughout the existing system, determining the chemical components, and modeling system, as shown in Fig. 1.

The initial 3D design was based on the average line representation, analyzed through CFD simulation to obtain a complete performance map and a reliable value cycle. The best thermodynamic cycle is the one that is most in sync with a given heat source. The Aspen Plus simulation results obtained the geometry of the OTEC Evaporator cycle shown in Fig. 1. The input parameters were used to obtain a different heat exchanger design with the overall OTEC cycle simulation. This aims to get a simpler design that will be easier to import and simulate.

This simulation study aims to then create a simulation model of the entire system made at Aspen Plus to determine the effect of some of the most important parameters, such as surface air temperature, deep sea water temperature and the difference in inlet temperature between surface and deep sea water through a heat exchanger. This article shows that compared to the initial design point, the total turbine power output after primary construction optimization, doubled and tripled, increased by 0.69 %, 1.82 % and 2.02 %, respectively. The optimal volume fraction, wheel diameter ratio and relative flow angle at the turbine rotor outlet after optimization of the triple construction are 0.243, 0.49 and 28°, respectively [18]. The total power output of the turbine will increase with increasing the inlet pressure of the low pressure turbine, the ratio of the mass flow rate of the working fluid. In this

paper, determine the optimal control system of a closed OTEC, carried out through simulation, compare the operating characteristics and to build a system that maintains a superheat of 1 °C or more according to changes in seawater temperature. The simulation results are sea surface temperature of 31 °C and seawater temperature of 5.5 °C, and changes in turbine output, flow rate, required power, and cooling pump evaporation pressure are compared as temperatures the difference is gradually decreasing.

The heat exchanger can thus be divided into three parts: preheating, evaporation, and overheating. So it is necessary to simulate two different designs, namely a heat exchanger with BEM type and a Heat Exchanger with BJM type. The points of variation that will be simulated can be seen in Fig. 2.

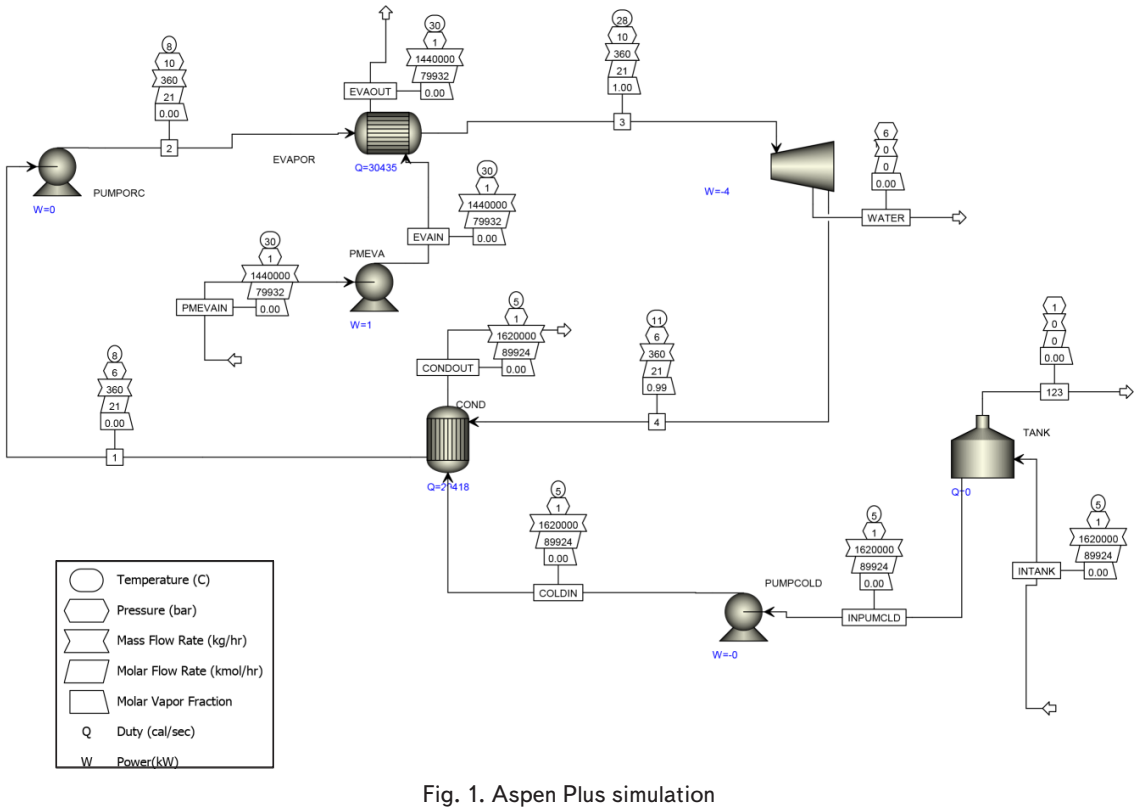

Fig. 1. Aspen Plus simulation

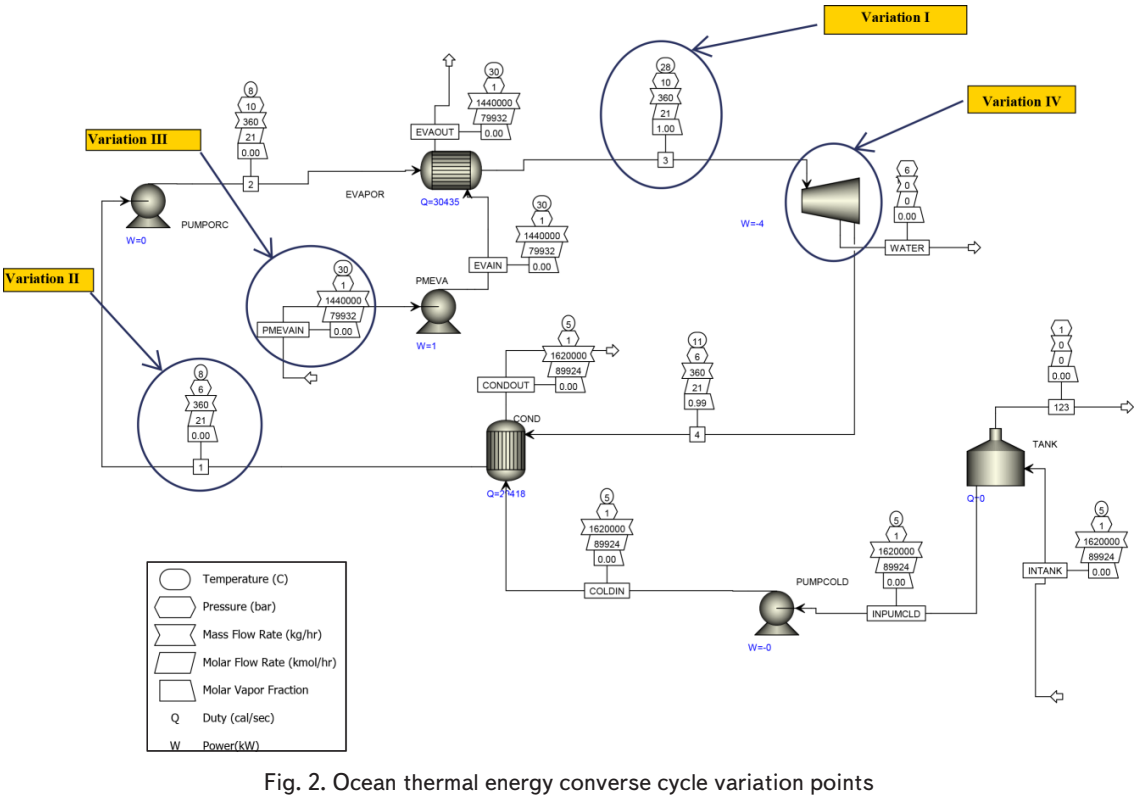

Fig. 2. Ocean thermal energy converse cycle variation points

The parameter values consisting of temperature, pressure, mass flow, and duty is a process to get 2 types of heat exchangers with different types. The geometric design is shown in Fig. 3 for the type of heat exchanger with the BEM type.

The concern about heat exchanger design that is too long indicates heat losses.

Whereas in a study of OTEC through solar collectors to simplify mathematical modeling, some assumptions have been made wherein heat loss in all pipes and fittings is negligible.

So a new design for the BJM type was made to compare with the BEM type, the design can be seen in Fig. 4.

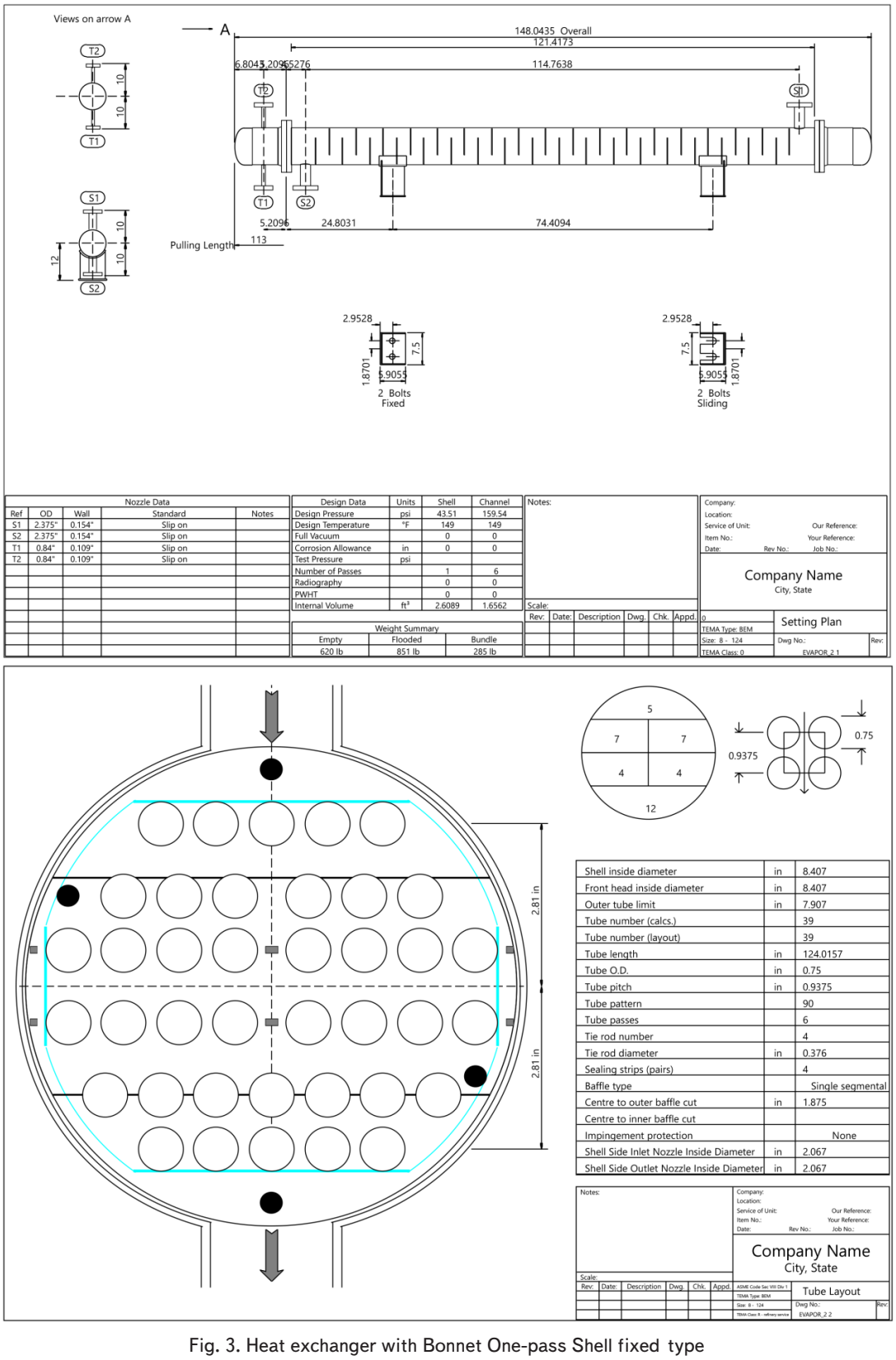

Nozzle Data				
Ref	OD	Wall	Standard	Notes
S1	2.375"	0.154"	Slip on	
S2	2.375"	0.154"	Slip on	
T1	0.84"	0.109"	Slip on	
T2	0.84"	0.109"	Slip on	

Design Data	Units	Shell	Channel
Design Pressure	psi	43.51	159.54
Design Temperature	°F	149	149
Full Vacuum		0	0
Corrosion Allowance	in	0	0
Test Pressure	psi		
Number of Passes		1	6
Radiography		0	0
PWHT		0	0
Internal Volume	ft³	2.6089	1.6562

Weight Summary		
Empty	Flooded	Bundle
620 lb	851 lb	285 lb

Shell inside diameter	in	8.407
Front head inside diameter	in	8.407
Outer tube limit	in	7.907
Tube number (calcs.)		39
Tube number (layout)		39
Tube length	in	124.0157
Tube O.D.	in	0.75
Tube pitch	in	0.9375
Tube pattern		90
Tube passes		6
Tie rod number		4
Tie rod diameter	in	0.376
Sealing strips (pairs)		4
Baffle type		Single segmental
Centre to outer baffle cut	in	1.875
Centre to inner baffle cut		
Impingement protection		None
Shell Side Inlet Nozzle Inside Diameter	in	2.067
Shell Side Outlet Nozzle Inside Diameter	in	2.067

Fig. 3. Heat exchanger with Bonnet One-pass Shell fixed type

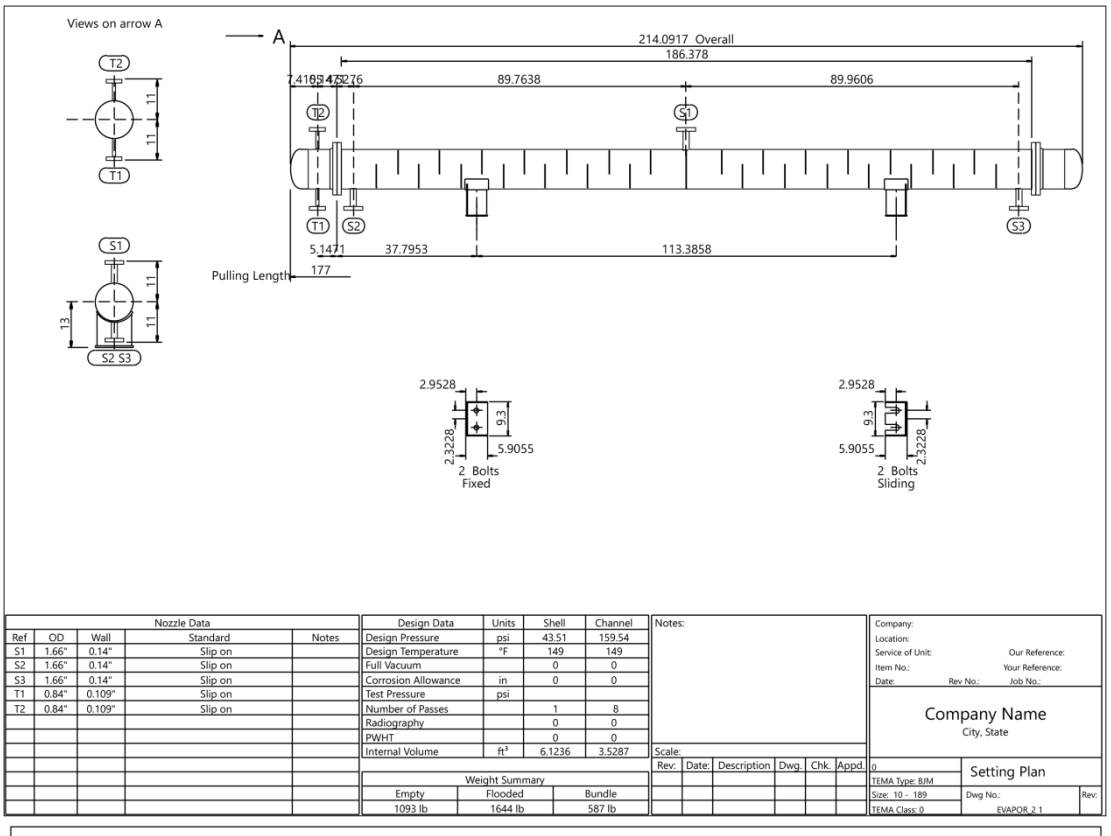

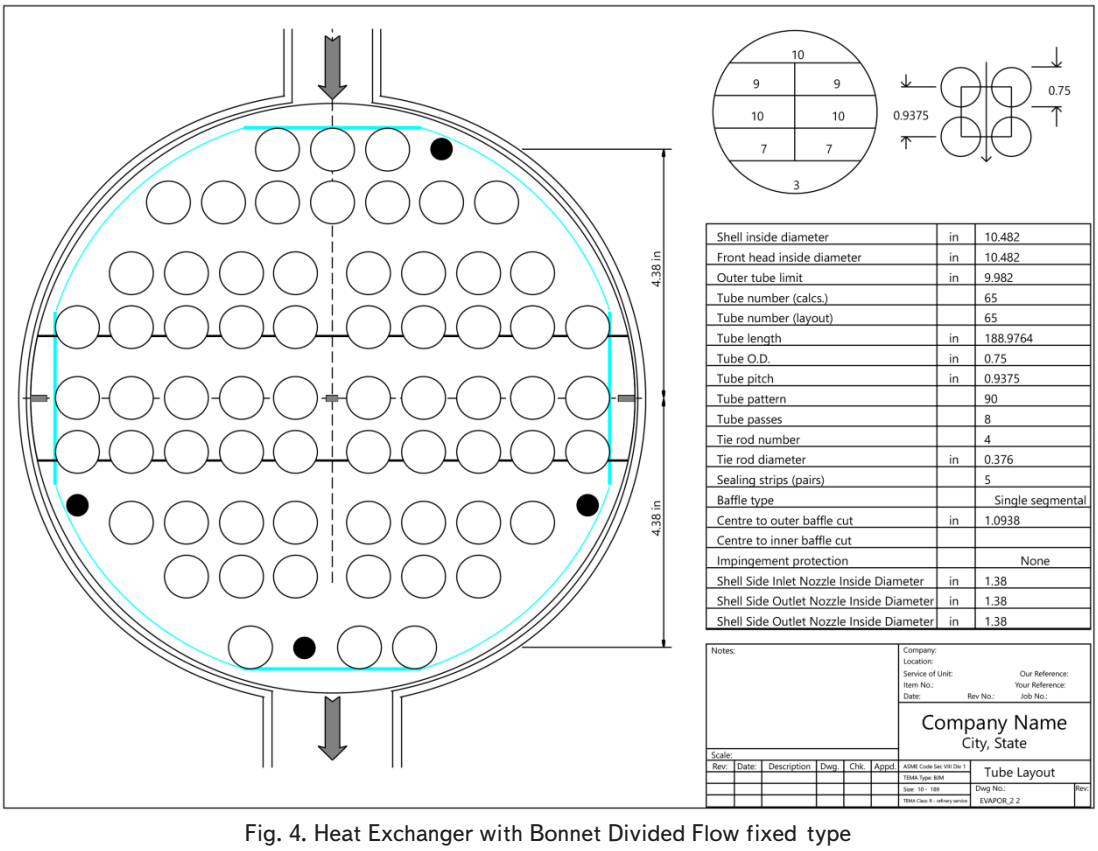

Fig. 4. Heat Exchanger with Bonnet Divided Flow fixed type

At this stage, monitoring of the OTEC system will be carried out using Aspen to investigate the effect of tin copper alloy's shell and tube evaporator heat exchanger system. The simulation setting in question is to determine several aspects needed in the simulation, such as the form of the selected solver, material, type of viscous, and others, according to the assumptions made. The predefined flow types are also set in this section within Fluent. The simulation is carried out by looking at the aspects in the form of solver models, viscous models, materials, operating conditions, initiation, and residual monitoring. Import geometry can be seen in Fig. 5.

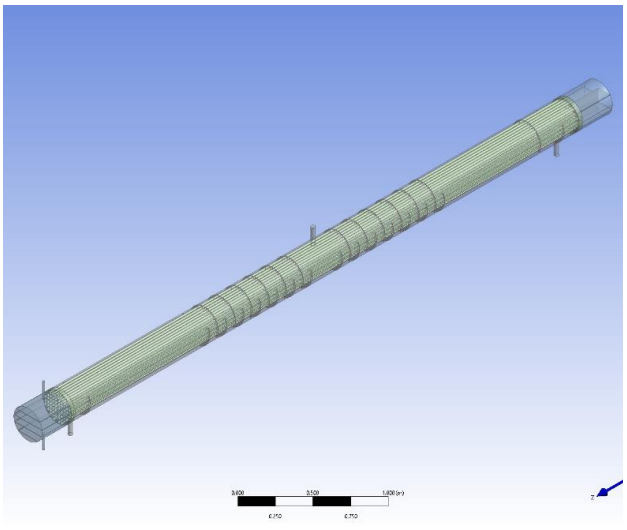

a

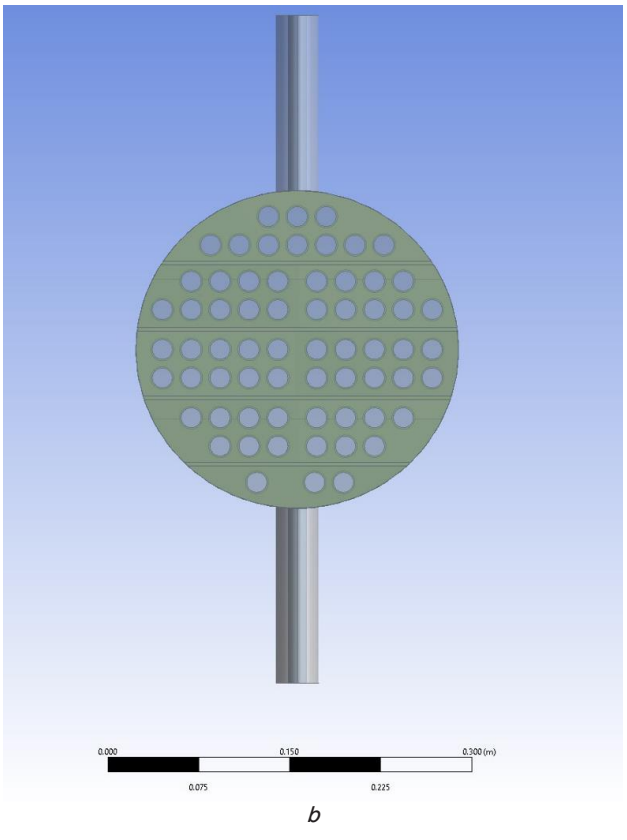

b

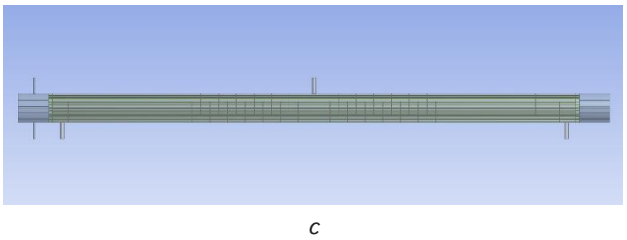

c

Fig. 5. Geometry Heat Exchanger Bonnet Divided Flow fixed: *a* — geometry; *b* — tubing positions; *c* — Buffle position

The Aspen Plus Simulation to CFD Simulation stage in this study aims to compare the results of the Heat Exchanger simulation design obtained from the Aspen Plus Software with the CFD simulation results. Import geometry can be seen in Fig. 6 type BEM.

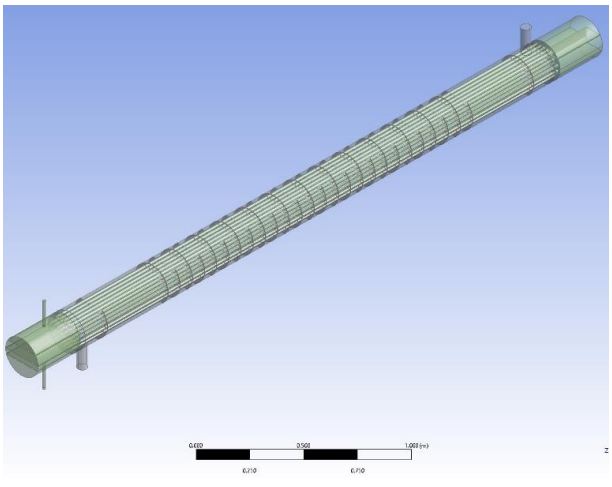

a

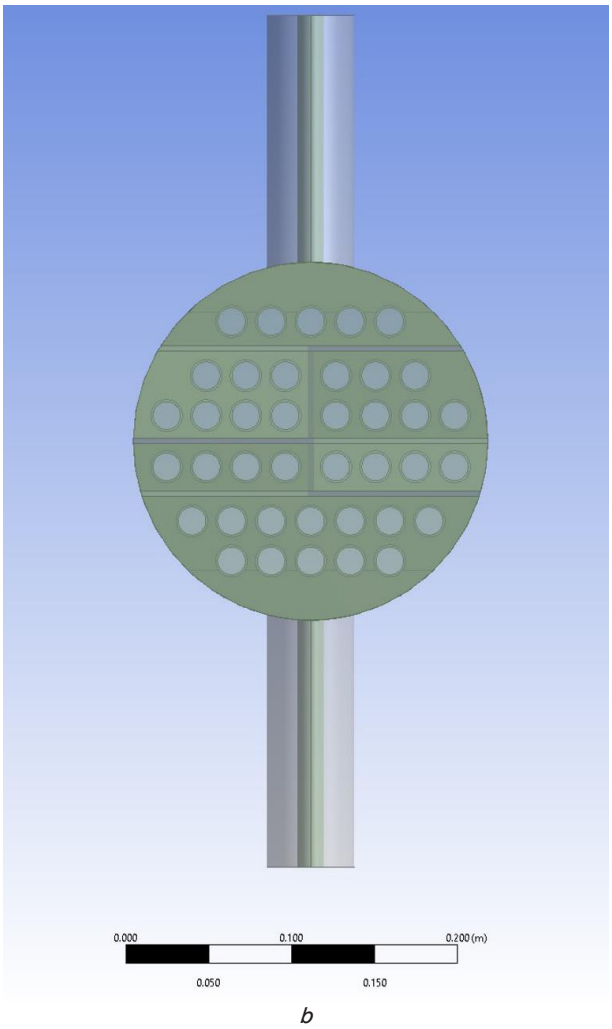

b

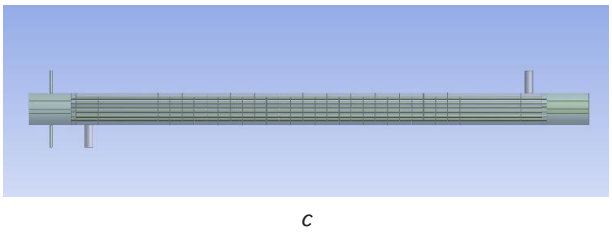

c

Fig. 6. Geometry Heat Exchanger type Bonnet One-pass Shell fixed: *a* — geometry; *b* — tubing position; *c* — buffle position

Meshing (grid generation) is obtained with 4 (four) mesh configurations to maintain the metric and ensure the difference in the results of the convergence criteria is less than 3 %. Volume units in the ANSYS simulation are interpreted by forming a mesh or grid. The mesh size applied to the model will affect the accuracy of the CFD analysis. The smaller the mesh size in the model, the more accurate the results will be, but it requires more computational power and time than larger mesh sizes. The profile obtained from the mesh used has a Tetrahedral type with the number of nodes=9,120,418 and the number of elements=5,206,956. The profile of the mesh can be seen in Fig. 7.

The large mesh size must be arranged in such a way (smooth meshing) so that accurate results are obtained and the computational power required is not too large, the following Fig. 8 is a BEM type meshing.

The boundary condition provides the initial input value and is useful for limiting the conditions during the process. The boundary conditions of this study are shown in Fig. 9 below.

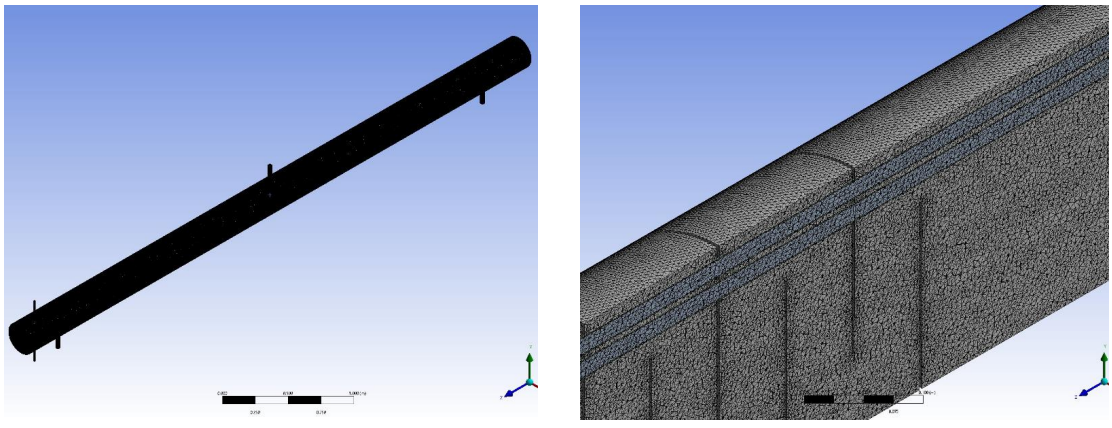

a *b*

Fig. 7. Meshing for type Bonnet Divided Flow fixed: *a* — tubing positions; *b* — meshing fix Support

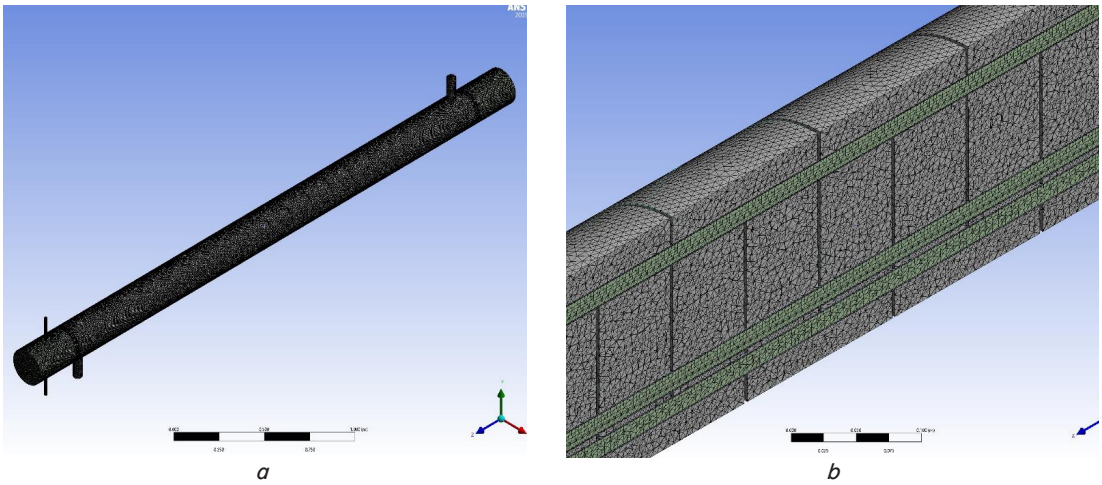

a *b*

Fig. 8. Meshing Heat Exchanger type Bonnet One-pass Shell fixed: *a* — tubing positions; *b* — meshing fix support

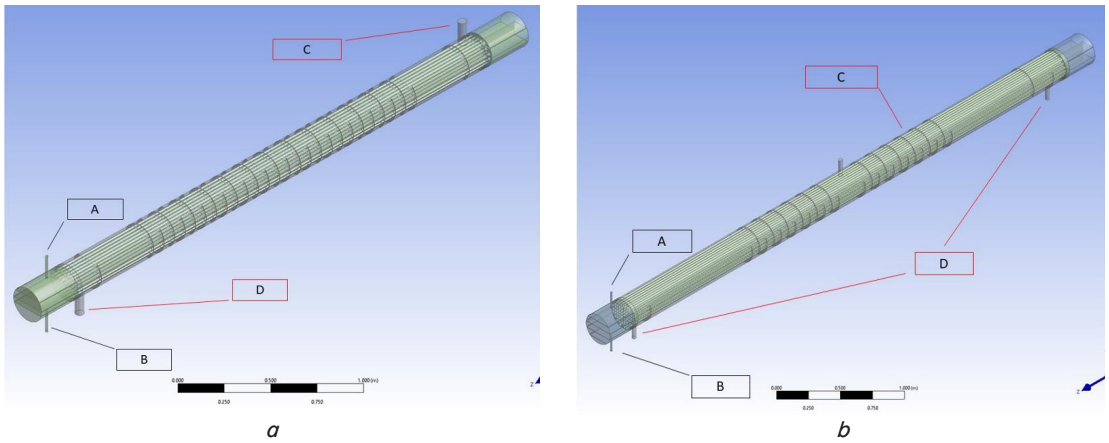

a *b*

Fig. 9. Simulation Boundary Conditions:
a — boundary condition Bonnet One-pass Shell fixed; *b* — boundary condition Bonnet Divided Flow fixed

There are 4 points, A, B, C, and D when determining simulation boundary conditions in BEM and BJM type heat exchangers. Point A inlet boundary conditions for ammonia are mass flow, inlet pressure, and inlet temperature. At point B, the type of ammonia outlet boundary condition is the outlet pressure. Point C determines the boundary conditions for inlet water, inlet pressure, and inlet temperature. At point D is the determination of the ammonia outlet. The following is a Table 1 of Aspen Plus simulation results for variation 1 of the evaporator exit temperature.

BEM type heat exchanger boundary conditions, types and values are listed in the Table 2 below.

The predefined flow types are also set in this section within FLUENT. The simulation is carried out by looking at the aspects in the form of solver models, viscous models, materials, operating conditions, initiation, and residual monitoring.

Table 1

Boundary condition BJM type

No.	Boundary Condition	Type	Value
A	Inlet Ammonia	Mass Flow	0.02 kg/s
	Pressure Inlet	Pressure Inlet	957.0 Pascal
	Temperature Inlet	Temperature	8 °C
B	Outlet Ammonia	Pressure Outlet	0 Pa (gauge)
C	Inlet Water	Mass Flow	0.02 kg/s
	Pressure Inlet	Pressure Inlet	1.015 Pascal
D	Temperature Inlet	Temperature	30 °C
	Outlet water	Pressure Outlet	0 Pa (gauge)

Table 2

Boundary condition heat exchanger BEM type

No.	Boundary Condition	Type	Value
A	Inlet Ammonia	Mass Flow	0.02 kg/s
	Pressure Inlet	Pressure Inlet	957.00Pascal
	Temperature Inlet	Temperature	8 °C
B	Outlet Ammonia	Pressure Outlet	0 Pa (gauge)
C	Inlet Water	Mass Flow	0.02 kg/s
	Pressure Inlet Temperature Inlet	Pressure Inlet Temperature	1.015 Pascal 30 °C
D	Outlet 1 water	Pressure Outlet	0 Pa (gauge)
	Outlet 2 water	Pressure Outlet	Pa (gauge)

5. Results of research on model variations and comparisons of simulations of heat exchangers for tin-copper alloys in the ocean thermal energy converse system

5. 1. Aspen Plus Simulation

The simulation results of these 4 variations use steady flow instead of transient Variation I, the initial evaporator exit temperature of this system built in Aspen Plus 24–29 °C is divided into 31 trials.

The following is Table 3 of Aspen Plus simulation results for variation 1 of the evaporator exit temperature.

Table 3

Simulation Results of Variation 1 Evaporator exit temperature

Row	Vary 1	*W* Pump Orc (kW)	*WM* evaporator (kW)	*Q* Evaporator (kW)	*Q* Condenser (kW)	*W* Turbine (kW)	*T* out Evaporator (°C)	*T* in Evaporator (°C)	*T* in Condenser (°C)	*T* out Condenser (°C)	*T* PM Evaporator in (°C)
1	24	0.08	1.06	126.5	122.3	4.2	29.9	29.9	4.99	5.0	30
2	24.1	0.08	1.06	126.6	122.3	4.2	29.9	29.9	4.99	5.0	30
3	24.3	0.08	1.06	126.6	122.4	4.2	29.9	29.9	4.99	5.0	30
4	24.5	0.08	1.06	126.6	122.4	4.2	29.9	29.9	4.99	5.0	30
5	24.6	0.08	1.06	126.7	122.5	4.2	29.9	29.9	4.99	5.0	30
6	24.8	0.08	1.06	126.7	122.5	4.3	29.9	29.9	4.99	5.0	30
7	25.0	0.08	1.06	126.8	122.5	4.3	29.9	29.9	4.99	5.0	30
8	25.2	0.08	1.06	126.8	122.6	4.3	29.9	29.9	4.99	5.0	30
9	25.3	0.08	1.06	126.8	122.6	4.3	29.9	29.9	4.99	5.0	30
10	25.5	0.08	1.06	126.9	122.6	4.3	29.9	29.9	4.99	5.0	30
11	25.7	0.08	1.06	126.9	122.7	4.3	29.9	29.9	4.99	5.0	30
12	25.8	0.08	1.06	126.9	122.7	4.3	29.9	29.9	4.99	5.0	30
13	26.0	0.08	1.06	127.0	122.7	4.3	29.9	29.9	4.99	5.0	30
14	26.2	0.08	1.06	127.0	122.8	4.3	29.9	29.9	4.99	5.0	30
15	26.4	0.08	1.06	127.0	122.8	4.3	29.9	29.9	4.99	5.0	30
16	26.5	0.08	1.06	127.1	122.8	4.3	29.9	29.9	4.99	5.0	30
17	26.7	0.08	1.06	127.1	122.9	4.3	29.9	29.9	4.99	5.0	30
18	26.9	0.08	1.06	127.2	122.9	4.3	29.9	29.9	4.99	5.0	30
19	27.1	0.08	1.06	127.2	122.9	4.3	29.9	29.9	4.99	5.0	30
20	27.2	0.08	1.06	127.2	123.0	4.3	29.9	29.9	4.99	5.0	30
21	27.4	0.08	1.06	127.3	123.0	4.3	29.9	29.9	4.99	5.0	30
22	27.6	0.08	1.06	127.3	123.0	4.3	29.9	29.9	4.99	5.0	30
23	27.7	0.08	1.06	127.3	123.1	4.3	29.9	29.9	4.99	5.0	30
24	27.9	0.08	1.06	127.4	123.1	4.3	29.9	29.9	4.99	5.0	30
25	28	0.08	1.06	127.4	123.1	4.3	29.9	29.9	4.99	5.0	30
26	28.1	0.08	1.06	127.4	123.1	4.3	29.9	29.9	4.99	5.0	30
27	28.3	0.08	1.06	127.4	123.2	4.3	29.9	29.9	4.99	5.0	30
28	28.4	0.08	1.06	127.5	123.2	4.3	29.9	29.9	4.99	5.0	30
29	28.6	0.08	1.06	127.5	123.2	4.3	29.9	29.9	4.99	5.0	30
30	28.8	0.08	1.06	127.5	123.3	4.3	29.9	29.9	4.99	5.0	30
31	29	0.08	1.06	127.6	123.3	4.3	29.9	29.9	4.99	5.0	30

It is known the value of the power of the evaporator, pump, and turbine, the capacity of the evaporator and condensate, and the outlet and inlet temperatures of the condensate and evaporator. From the simulation results of variation 1, graphically, is possible to see in Fig. 10.

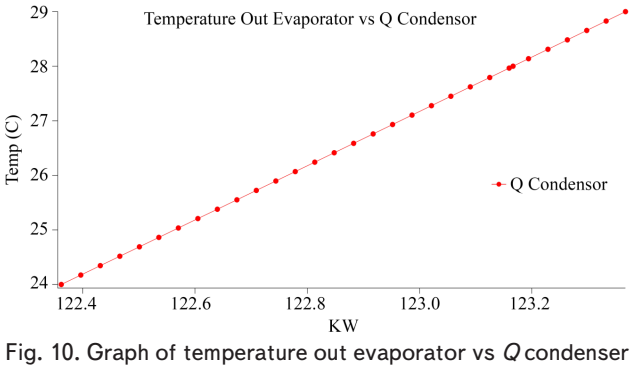

Fig. 10. Graph of temperature out evaporator vs *Q* condenser

It can be seen that the higher the output temperature out from the evaporator, the higher (*Q*) obtained from the condenser. The results can be seen in the graph in Fig. 11.

In the graph in Fig. 12 below, the evaporator output temperature it can be concluded that the higher the output temperature at the evaporator, the higher the *W* Turbine absorbed by the evaporator.

In variation II, the initial condenser exit temperature of this system which has been built at Aspen Plus 6–10 °C is divided into 31 experiments. Table 4 Simulation Results for Variation II resulted in the exit temperature of the condenser vs. *Q* of the condenser, the exit temperature of the condenser vs. the *W* Pump of the evaporator, and the exit temperature of the condenser vs. the *Q* of the evaporator.

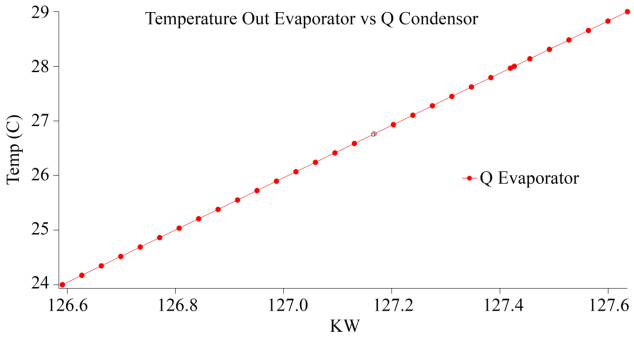

Fig. 11. Graph of temperature out evaporator vs *Q* evaporator

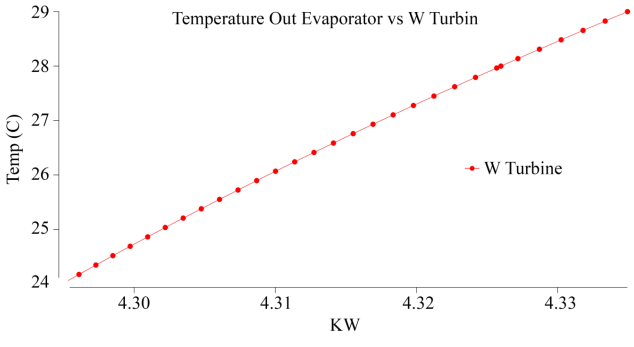

Fig. 12. Graph of temperature out evaporator vs *W* turbine

Table 4

Simulations resulted in variation II exit temperature of condenser vs Q of the condenser

No.	Vary 1 Condenser Hot (C)	*W* Pump Orc (kW)	*WM* Evaporator (kW)	*Q* Evaporator (kW)	*Q* Condenser (kW)	*W* Turbine (kW)	*T* out Evaporator (°C)	*T* in Evaporator (°C)	*T* in Condenser (°C)	*T* out Condenser (°C)	*T* in Evaporator (°C)
1	6.0	0.08	1.0	128.6	124.3	4.3	29.9	29.9	4.99	5.06	30
2	6.1	0.08	1.0	128.5	124.2	4.3	29.9	29.9	4.99	5.06	30
3	6.3	0.08	1.0	128.6	124.1	4.3	29.9	29.9	4.99	5.06	30
4	6.4	0.08	1.0	128.3	124.0	4.3	29.9	29.9	4.99	5.06	30
5	6.5	0.08	1.0	128.2	124.0	4.3	29.9	29.9	4.99	5.06	30
6	6. 7	0.08	1.0	128.1	123.9	4.3	29.9	29.9	4.99	5.06	30
7	6.8	0.08	1.0	128.1	123.8	4.3	29.9	29.9	4.99	5.06	30
8	6.9	0.08	1.0	128.0	123.7	4.3	29.9	29.9	4.99	5.06	30
9	7.1	0.08	1.0	127.9	123.6	4.3	29.9	29.9	4.99	5.06	30
10	7.2	0.082	1.0	127.8	123.6	4.3	29.9	29.9	4.99	5.06	30
11	7.4	0.08	1.0	127.7	123.5	4.3	29.9	29.9	4.99	5.06	30
12	7.5	0.08	1.0	127.7	123.4	4.3	29.9	29.9	4.99	5.06	30
13	7.6	0.08	1.0	127.6	123.3	4.3	29.9	29.9	4.99	5.06	30
14	7.8	0.08	1.0	127.5	123.2	4.3	29.9	29.9	4.99	5.06	30
15	7.9	0.08	1.0	127.4	123.2	4.3	29.9	29.9	4.99	5.06	30
16	8.0	0.08	1.0	127.4	123.1	4.3	29.9	29.9	4.99	5.06	30
17	8.1	0.08	1.0	127.3	123.1	4.3	29.9	29.9	4.99	5.06	30
18	8.2	0.08	1.0	127.3	123.0	4.3	29.9	29.9	4.99	5.06	30
19	8.3	0.08	1.0	127.2	122.9	4.3	29.9	29.9	4.99	5.06	30
20	8.4	0.08	1.05	127.1	122.8	4.3	29.9	29.9	4.99	5.06	30
21	8.6	0.08	1.0	127.0	122.8	4.3	29.9	29.9	4.99	5.06	30
22	8.7	0.08	1.0	126.9	122.7	4.3	29.9	29.9	4.99	5.06	30
23	8.8	0.08	1.0	126.9	122.6	4.3	29.9	29.9	4.99	5.06	30
24	9.0	0.08	1.0	126.8	122.5	4.3	29.9	29.9	4.99	5.06	30
25	9.2	0.08	1.0	126.7	122.4	4.3	29.9	29.9	4.99	5.06	30
26	9.3	0.08	1.0	126.6	122.4	4.3	29.9	29.9	4.99	5.064	30
27	9.4	0.08	1.0	126.5	122.3	4.3	29.9	29.9	4.99	5.06	30
28	9.6	0.08	1.0	126.5	122.2	4.3	29.9	29.9	4.99	5.06	30
29	9.7	0.08	1.0	126.4	122.1	4.3	29.9	29.9	4.99	5.06	30
30	9.9	0.08	1.0	126.3	122.0	4.3	29.9	29.9	4.99	5.06	30
31	10	0.08	1.0	126.2	122.0	4.3	29.9	29.9	4.99	5.06	30

The condenser outlet temperature was lowered from 10–60 °C divided into 31 experiments. The red part is a variation. The lower the output temperature of the condenser, the lower the Q of the condenser as well. The heat released is getting lower also at different characters in each component. The graph can be seen in Fig. 13.

Fig. 14 shows the higher the exit temperature of the condenser, the higher the power (*W*) of the pump in the evaporator. In the field case, the higher the pump output power, the heavier the pump performance. The pump works lower then the condenser *Q* is lower or the pump specifications are increased in power.

Fig. 15 concluded that if the *Q* of the evaporator is low, the temperature coming out of the condenser is also low. The temperature value issued by one of the components in this OTEC system greatly affects the other components.

The results of the simulation of Variation III will be tested, and the resulting conditions for the mass flow rate of the heating water to the temperature coming out of the evaporator. Furthermore, data on the effect of the mass flow rate of heating water on the power (*W*) of the pump in the evaporator is also generated.

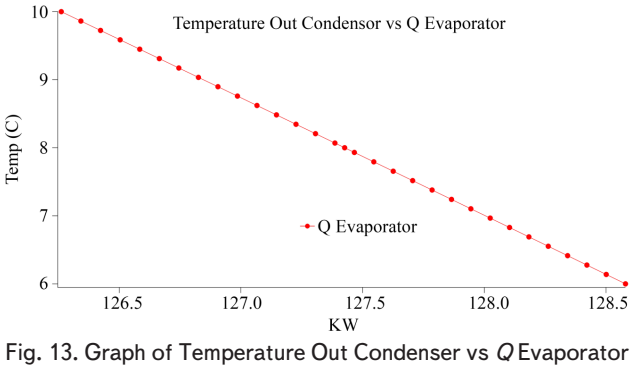

Fig. 13. Graph of Temperature Out Condenser vs *Q* Evaporator

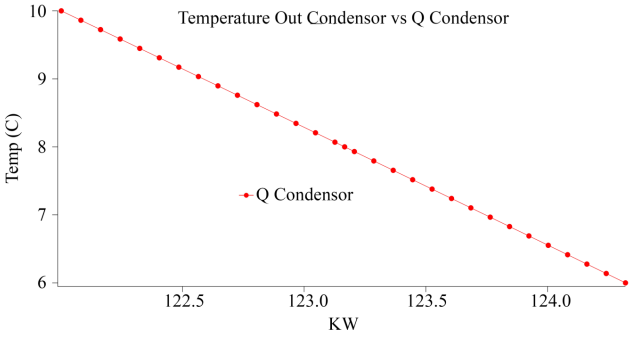

Fig. 14. Graph of Temperature Out Condenser vs *Q* Condenser

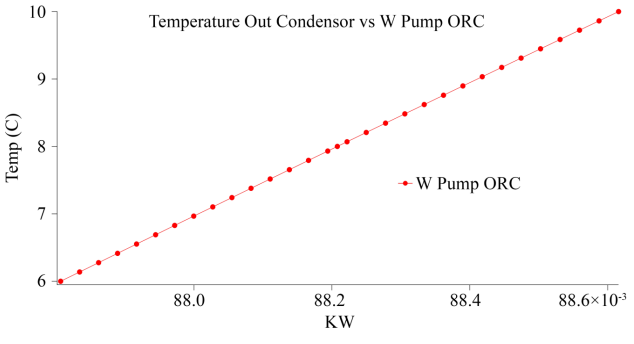

Fig. 15. Graph of Evaporator Out Temperature vs *W* Pump Evaporator

The results of the simulation of Variation III will be tested and the resulting conditions for the mass flow rate of the heating water to the temperature coming out of the evaporator. The results of the aspen plus simulation analysis in the variation III simulation can be seen in Table 5.

Table 5

Simulation Results of Variation III Mass Flow Rate from Sea Surface, PM Evaporator in Mixed HO Mass flow

No	VARY 1	*W* Pump Orc (kW)	*WM* Evaporator (kW)	*Q* Evaporator (kW)	*Q* Condenser (kW)	*W* Turbine (kW)	*T* out Evaporator (°C)	*T* in Evaporator (°C)	*T* in Condenser (°C)	*T* out Condenser (°C)	*PM* Evaporator (°C)
1	720000	0.08	0.53	127.4	123.1	4.3	29.8	29.8	4.9	5.06	30
2	744827.6	0.08	0.54	127.4	123.1	4.3	29.8	29.8	4.9	5.06	30
3	769655.2	0.08	0.56	127.4	123.1	4.3	29.8	29.8	4.9	5.06	30
4	794482.8	0.08	0.58	127.4	123.1	4.3	29.8	29.8	4.9	5.06	30
5	819310.3	0.08	0.60	127.4	123.1	4.3	29.8	29.8	4.9	5.06	30
6	844137.9	0.08	0.62	127.4	123.1	4.3	29.8	29.8	4.9	5.06	30
7	868965.5	0.08	0.63	127.4	123.1	4.3	29.8	29.8	4.9	5.06	30
8	893793.1	0.08	0.65	127.4	123.1	4.3	29.8	29.8	4.9	5.06	30
9	918620.7	0.08	0.67	127.4	123.1	4.3	29.8	29.8	4.9	5.06	30
10	943448.3	0.08	0.69	127.4	123.1	4.3	29.8	29.8	4.9	5.06	30
11	968275.9	0.08	0.71	127.4	123.1	4.3	29.8	29.8	4.9	5.06	30
12	993103.4	0.08	0.72	127.4	123.1	4.3	29.8	29.8	4.9	5.06	30
13	1017931	0.08	0.74	127.4	123.1	4.3	29.8	29.8	4.9	5.06	30
14	1042759	0.08	0.76	127.4	123.1	4.3	29.8	29.8	4.9	5.06	30
15	1067586	0.08	0.78	127.4	123.1	4.3	29.8	29.8	4.9	5.06	30
16	1092414	0.08	0.80	127.4	123.1	4.3	29.8	29.8	4.9	5.06	30
17	1117241	0.08	0.82	127.4	123.1	4.3	29.9	29.9	4.9	5.06	30
18	1142069	0.08	0.83	127.4	123.1	4.3	29.9	29.9	4.9	5.06	30
19	1166897	0.08	0.852	127.4	123.1	4.3	29.9	29.9	4.9	5.06	30
20	1191724	0.08	0.87	127.4	123.1	4.3	29.9	29.9	4.9	5.06	30
21	1216552	0.08	0.89	127.4	123.1	4.3	29.9	29.9	4.9	5.06	30
22	1241379	0.08	0.91	127.4	123.1	4.3	29.9	29.9	4.9	5.06	30
23	1266207	0.08	0.930	127.4	123.1	4.3	29.9	29.9	4.9	5.06	30
24	1291034	0.08	0.94	127.4	123.1	4.3	29.9	29.9	4.9	5.06	30
25	1315862	0.08	0.96	127.4	123.1	4.3	29.9	29.9	4.9	5.06	30
26	1340690	0.08	0.98	127.4	123.1	4.3	29.9	29.9	4.9	5.06	30
27	1365517	0.08	1.00	127.4	123.1	4.3	29.9	29.9	4.9	5.06	30
28	1390345	0.08	1.02	127.4	123.1	4.3	29.9	29.9	4.9	5.06	30
29	1415172	0.08	1.04	127.4	123.1	4.3	29.9	29.9	4.9	5.06	30
30	1440000	0.08	1.05	127.4	123.1	4.3	29.9	29.9	4.9	5.06	30

Fig. 16 shows that the higher the exit temperature of the evaporator, the higher the heating water mass flow rate, where the mass flow rate (kg/h) shows an increase.

Fig. 17 show the flow rate of heating water will greatly affect the power (*W*) of the evaporator pump.

Simulation on variation IV of turbine outlet pressure, where the analysis of ammonia VS *T* out turbine pressure, ammonia VS *T* out condenser pressure, Ammonia pressure vs Condenser *Q*. Starting at 6.25 bar for up to 30 simulation times and delivering up to 8.0 bar. Thereby affecting other components.

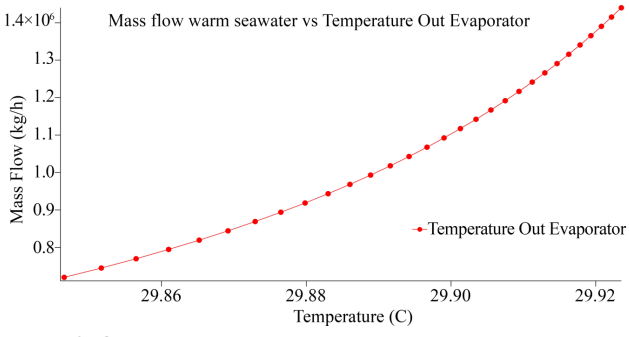

Fig. 16. Graph of mass flow warm seawater vs temperature out the evaporator

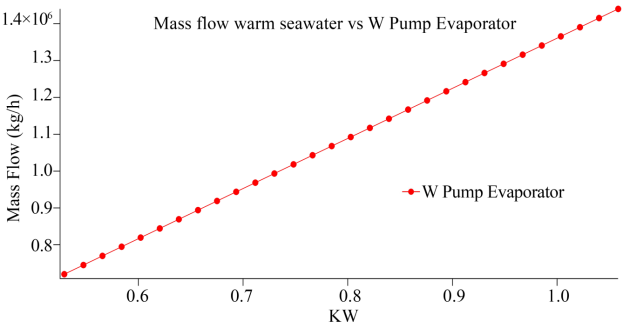

Fig. 17. Graph of mass flow warm seawater vs *W* pump evaporator

The results of the simulation on variation IV of turbine outlet pressure, which analyzed the ammonia VS *T* out turbine pressure, ammonia VS *T* out condenser pressure, and Ammonia pressure with *Q* condenser. Starting at 6.25 bar for up to 30 simulation times and delivering up to 8.0 bar thus affecting other components.

Fig. 18 shows that ammonia is proportional to the exit temperature of the turbine. The red mark is the turbine exit pressure, the higher the pressure in the ammonia working fluid, the higher the turbine exit temperature.

Table 6

Simulation Results of Variation IV Turbine Out Pressure

No.	Vary 1	*W* Pump Orc (kW)	*Wm* Evaporator (kW)	*Q* Evaporator (kW)	*Q* Condenser (kW)	*W* Turbine (kW)	*T* out Evaporator (°C)	*T* in Evaporator (°C)	*T* in Condenser (°C)	*T* out Condenser (°C)	*T* Pm Evaporator in (°C)	*T* out Turbine (°C)
1	6.25	0.088	1.05	127.2	123.1	4.3	29.9	29.9	4.9	5.06	30	10.5
2	6.31	0.086	1.05	127.2	123.2	4.2	29.9	29.9	4.9	5.06	30	10.8
3	6.37	0.085	1.05	127.2	123.3	4.1	29.9	29.9	4.9	5.06	30	11.1
4	6.43	0.083	1.05	127.3	123.4	4.0	29.9	29.9	4.9	5.06	30	11.3
5	6.49	0.081	1.05	127.3	123.5	3.9	29.9	29.9	4.9	5.06	30	11.6
6	6.55	0.080	1.05	127.3	123.6	3.8	29.9	29.9	4.9	5.06	30	11.9
7	6.61	0.078	1.05	127.3	123.7	3.7	29.9	29.9	4.9	5.06	30	12.2
8	6.67	0.076	1.05	127.3	123.8	3.6	29.9	29.9	4.9	5.06	30	12.4
9	6.73	0.075	1.05	127.3	123.8	3.5	29.9	29.9	4.9	5.06	30	12.7
10	6.79	0.073	1.05	127.3	123.9	3.5	29.9	29.9	4.9	5.06	30	13,0
11	6.85	0.072	1.05	127.4	124.0	3.4	29.9	29.9	4.9	5.06	30	13.2
12	6.91	0.070	1.05	127.4	124.1	3.3	29.9	29.9	4.9	5.06	30	13.5
13	6.97	0.068	1.05	127.4	124.2	3.2	29.9	29.9	4.9	5.06	30	13.7
14	7.03	0.067	1.05	127.4	124.3	3.1	29.9	29.9	4.9	5.06	30	14.0
15	7.09	0.065	1.05	127.4	124.4	3.0	29.9	29.9	4.9	5.06	30	14.2
16	7.15	0.064	1.05	127.4	124.5	2.9	29.9	29.9	4.9	5.06	30	14.5
17	7.21	0.062	1.05	127.4	124.5	2.9	29.9	29.9	4.9	5.06	30	14.8
18	7.27	0.060	1.05	127.4	124.6	2.8	29.9	29.9	4.9	5.06	30	15.0
19	7.33	0.059	1.05	127.4	124.7	2.7	29.9	29.9	4.9	5.06	30	15.3
20	7.39	0.057	1.05	127.4	124.8	2.6	29.3	29.9	4.9	5.06	30	15.5
21	7.45	0.056	1.05	127.4	124.9	2.5	29.9	29.9	4.9	5.06	30	15.7
22	7.51	0.054	1.05	127.4	125.0	2.4	29.9	29.9	4.9	5.06	30	16.0
23	7.57	0.052	1.05	127.4	125.0	2.4	29.9	29.9	4.9	5.06	30	16.4
24	7.63	0.051	1.05	127.4	125.1	2.3	29.9	29.9	4.9	5.06	30	16.8
25	7.69	0.049	1.05	127.4	125.2	2.2	29.9	29.9	4.9	5.06	30	17.2
26	7.75	0.048	1.05	127.4	125.3	2.1	29.9	29.9	4.9	5.06	30	17.5
27	7.81	0.046	1.05	127.4	125.4	2.0	29.9	29.9	4.9	5.06	30	17.9
28	7.87	0.044	1.05	127.4	125.4	2.0	29.9	29.9	4.9	5.06	30	18.3
29	7.93	0.043	1.05	127.4	125.5	1.9	29.9	29.9	4.9	5.06	30	18.7
30	8	0.041	1.05	127.4	125.6	1.8	29.9	29.9	4.9	5.06	30	19.0

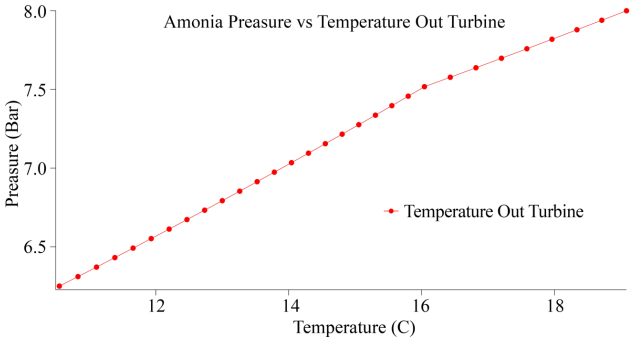

Fig. 18. Ammonia Pressure vs *T* out Turbine

In Fig. 19, the vapor pressure of ammonia is proportional to the exit temperature of the condenser. The results show that the higher the vapor pressure in the ammonia, the temperature at the exit temperature of the condenser also increases from 6.0 bar – 8.0 bar, while the temperature at the exit of the condenser increases from 5.0674 °C – 5.0684 °C.

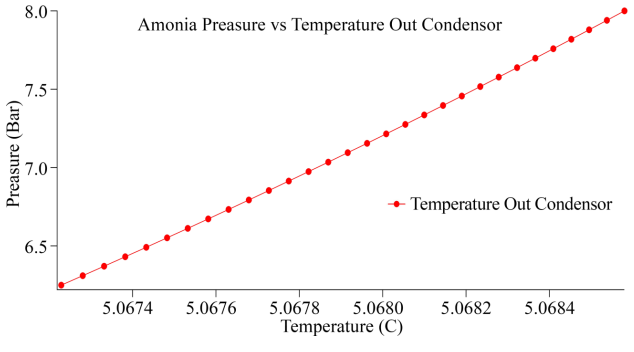

Fig. 19. Ammonia Pressure vs Temperature Out Condenser

The graph in Fig. 20. shows the ammonia pressure compared to the capacity (*Q*) out of the condenser. The result is that the higher the vapor pressure in the ammonia, the higher the capacity (*Q*) coming out of the condenser from 6.0 bar – 8.0 bar, while the capacity (*Q*) coming out of the condenser increases from 123.5 kW – 125.5 kW.

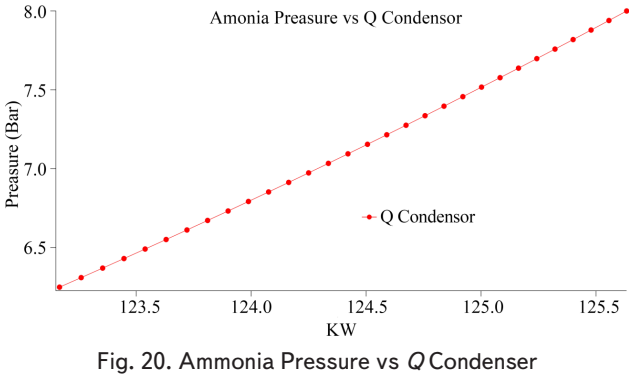

Fig. 20. Ammonia Pressure vs *Q* Condenser

The graph in Fig. 21 shows that the higher the ammonia pressure, the conditions in the evaporator Capacity (*Q*) area will also increase. Ammonia pressure 6.0 bar to 8.0 bar along with the increase in *Q* evaporator from 127.4 kW.

The graph in Fig. 22 decreases the vapor pressure of ammonia, so it affects the power increase in the ORC pump. Ammonia pressure from 8 bar decreases to 6.0 bar at *W* Pump ORC.

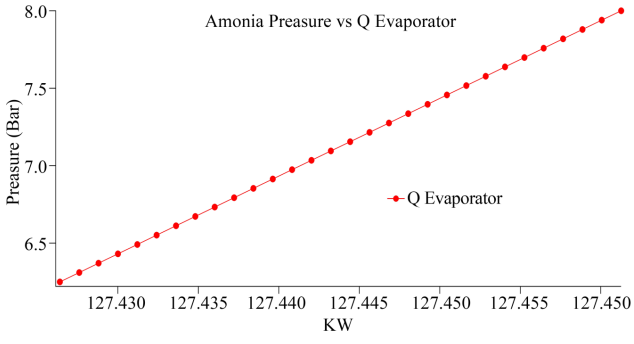

Fig. 21. Ammonia Pressure vs *Q* Evaporator

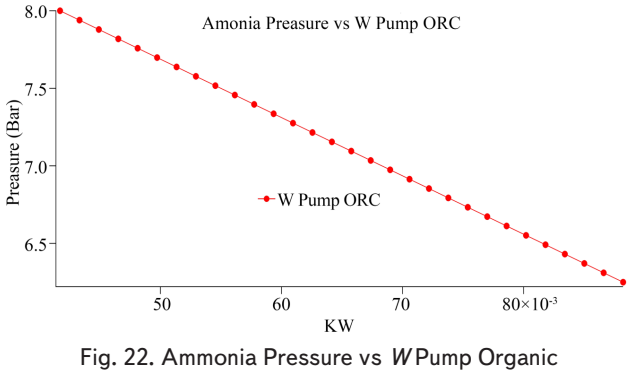

Fig. 22. Ammonia Pressure vs *W* Pump Organic Rankine Cycle

If the pressure of the ammonia vapor produced after going through the heating process in the evaporator decreases, then the power (*W*) of the turbine power also increases. From the graph, it is read that the steam pressure is 8.0 bar – 6.0 bar after going through the heating process but the power has increased from 2.0 kW – 4.0 kW. The results of the graph can be seen in Fig. 23.

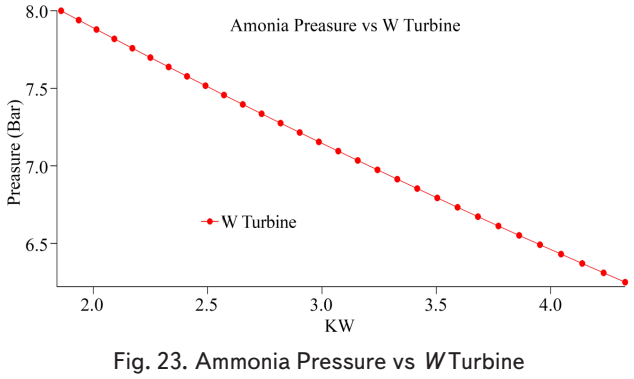

Fig. 23. Ammonia Pressure vs *W* Turbine

The overall Aspen Plus simulation results, from variation I to variation IV, are summarized in the summary table and will be compared with the results of the ANSYS CFD.

5. 2. Ansys Computational Fluid Dynamics Simulation of Heat Exchanger Bonnet Divided Flow fixed Type

The ANSYS CFD process for the BJM type Heat Exchanger simulation results can be seen in the input parameters. Hot water inlet at sea level where water enters the evaporator when it exits the evaporator and at the ammonia inlet line the inlet temperature and outlet temperature. The CFD Contour Temperature BJM simulation results show the obtained temperature value shown in Fig. 24.

The Ansys CFD simulation seen from the pressure contour side is almost the same as the reading on the temperature contour. The more the color leads to the red distribution, the higher the pressure values on the heat exchanger component can be seen in Fig. 25.

Fig. 26 shows the position of the BEM type CFD pressure contour which is almost the same as the CFD temperature contour (BJM). The more the color leads to the red distribution, the higher the pressure values on the Heat Exchanger component.

Fig. 27 geometry with the SolidWorks application, if it has been completed then the continuation of the image is imported to Ansys CFD on the Ansys application network to determine the temperature of both the heating water from the sea surface and the temperature of the ammonia working fluid, especially HE building is necessary.

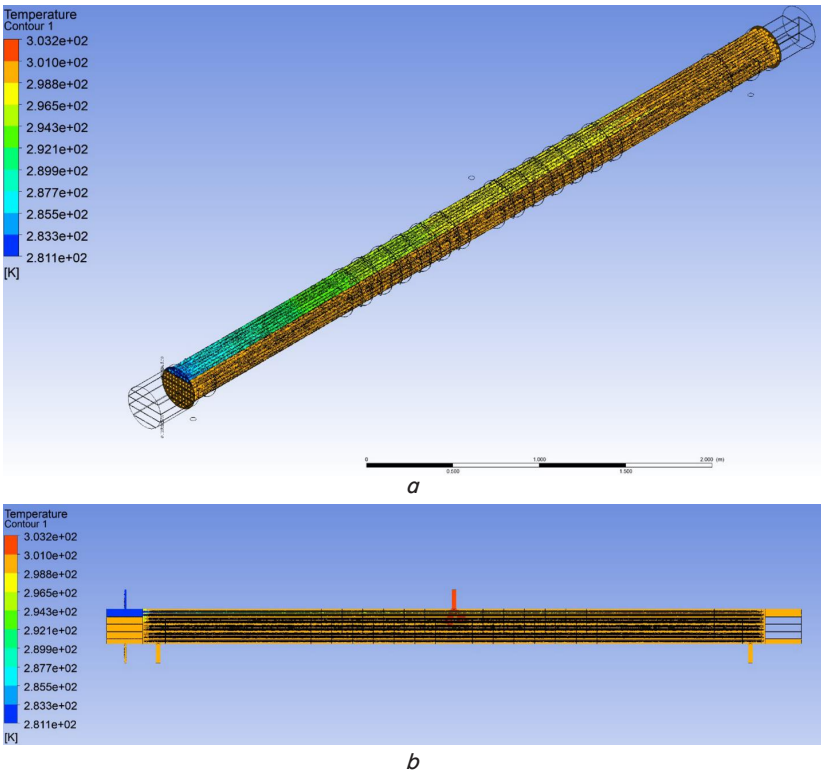

Fig. 24. Ansys Computational Fluid Dynamics simulation Bonnet Divided Flow fixed type: *a* — buffle shape; *b* — contour temperature

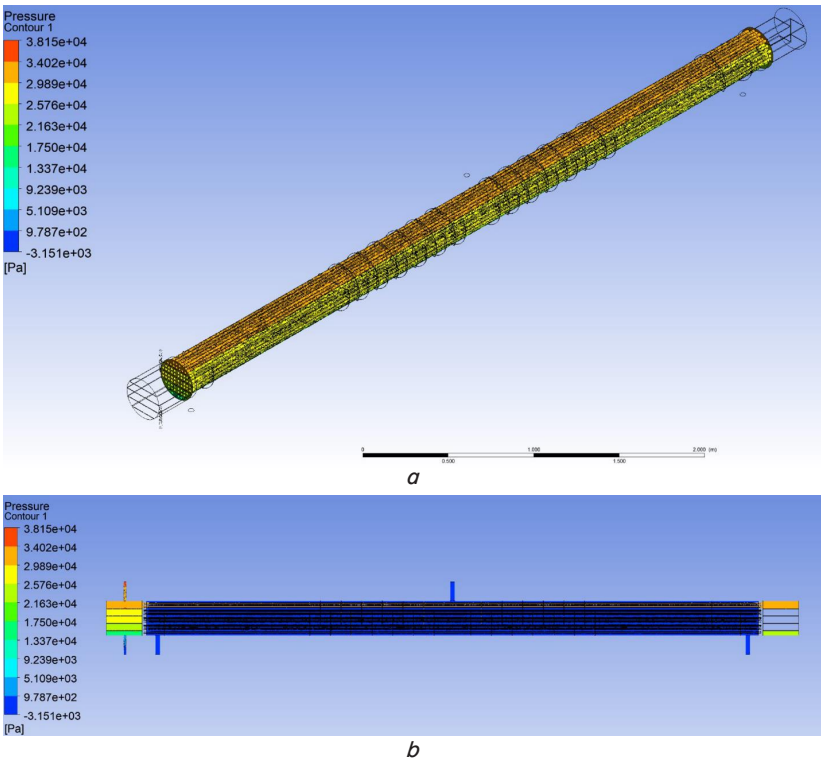

Fig. 25. Computational Fluid Dynamics simulation Bonnet Divided Flow fixed type *a* — contour pressure; *b* — buffle shape

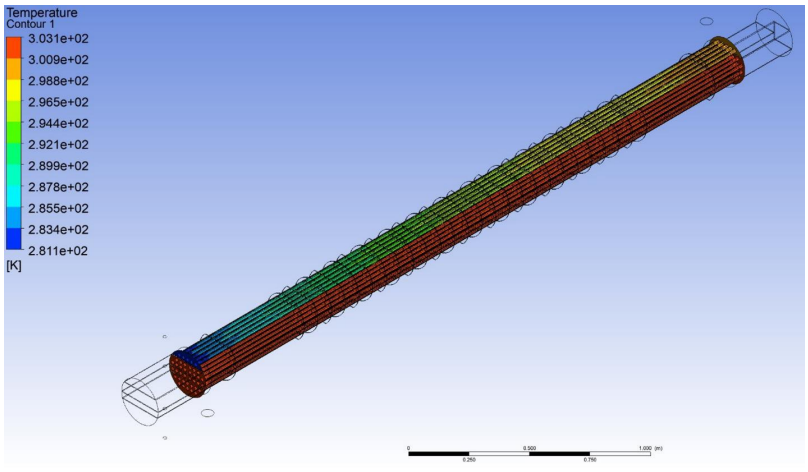

a

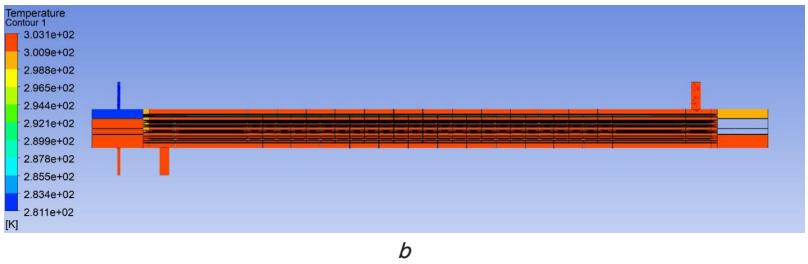

b

Fig. 26. Computational Fluid Dynamics simulation Bonnet Divided Flow fixed type: *a* — temperature contour (BEM); *b* — buffle shape

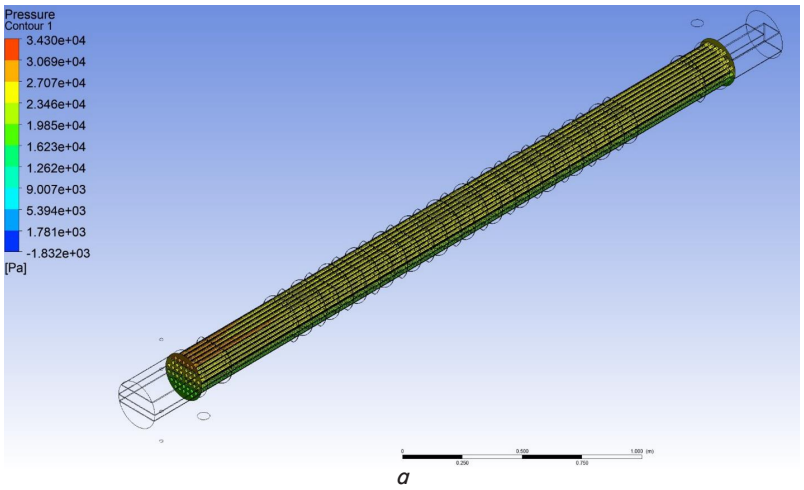

a

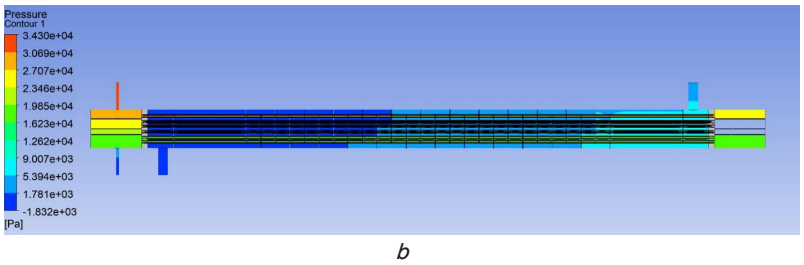

b

Fig. 27. Computational Fluid Dynamics Pressure Contour: *a* — pressure contour; *b* — buffle shape

The more the color leads to the red distribution, the higher the pressure values on the heat exchanger component, the distribution of pressure values in the pipe begins with the entry of ammonia pressure, the blue mark is at a temperature of –1.832 Pa until the heat exchanger exits with a red mark indicating a temperature of 3.43 Pa. The flow of working fluid in the heat exchanger occurs several times back and forth, not just one turn, after which the heat exchanger comes out.

5. 3. Comparison of Computational Fluid Dynamics Simulation and Aspen Plus

The results of the comparison of CFD and Aspen Plus simulations on BJM and BEM type Heat Exchangers are clearly shown in Tables 7, 8 below.

Aspen Plus and Ansys CFD applications have been completed and simulated and produce both the temperature of the heating water from sea level and the temperature of the

ammonia working fluid. This type of BEM heat exchange is a top priority in investigating the large temperature and pressure that occurs, with the initial design model without the input inlet hole in the middle, which is the opposite of the BJM type which uses a supporting inlet in the middle. The distribution of pressure values in the pipe begins with the entry of the ammonia pressure with the blue mark and the exit of the Heat Exchanger with the red mark that the comparison results of CFD and Aspen Plus simulations on BJM type HE and BEM type HE, the best design is in the BEM type both in terms of working fluid and heating water. With values listed in Tables 7, 8, at least they can design and recommend experimental tests by making a prototype heat exchanger model.

Table 7

Comparison of CFD and Aspen Plus HE Type BJM simulation results

Type	Parameter	Temperature (°C)	
		Aspen Plus Simulation	CFD Simulation
BJM	Ammonia Inlet	8 °C	7.99 °C
	Heating Water Inlet	30 °C	29.99 °C
	Ammonia Outlet	28 °C	26.30 °C
	Heating Water Outlet	28 °C	26.31 °C

Table 8

Comparison of CFD and Aspen Plus Heat Exchanger Type BEM

Type	Parameter	Temperature (°C)	
		Aspen Plus Simulation	CFD Simulation
BEM	Ammonia Inlet	8 °C	7.99 °C
	Heating Water Inlet	30 °C	29.99 °C
	Ammonia Outlet	28 °C	28.21 °C
	Heating Water Outlet	28 °C	28.15 °C

6. Discussion of Results of research on model variations and comparisons of simulations of heat exchangers for tin-copper alloys in the ocean thermal energy converse system

Interpreted by analyzing the results (Fig. 24–27) heat exchanger with copper tin alloy material has been subjected to friction in the shell and tube space. The interaction between ammonia and hot water produces varying temperature outputs, BEM type 30 °C is greater than BJM type 26 °C. Overall it can be claimed that the heat loss in the BJM type is due to turbulence at the hot water inlet at the center of the heat exchanger.

Copper tin alloy in the OTEC heat exchanger system is capable of producing saturated steam which is expected to turn a turbine with a power output of 4 KW.

The limitation of this research is that it is still limited to the working fluid of ammonia, perhaps it can be varied with other working fluids.

Compared to titanium material which is quite expensive, this heat exchanger tin copper alloy BEM type can be recommended to be prototyped as a comparison with simulation results for the future.

As an alternative to the manufacture of OTEC factories in Indonesia, Tin Copper material can be recommended as a Heat Exchanger and can also be discussed in the future in the mathematics section in combination with material properties to determine the characteristics of materials in the sea.

Against previous studies where good results were achieved, it is possible to conclude Regarding e, this work achieves lower scores than other jobs: 2.42 % (for 2 R1234yf), 2.40 % (for ammonia) and 2.27 % (for decafluorobutane). 2.75 % and 3.06 % for ammonia 4 and R423a, respectively. The lowest ε value of this work is mainly explained by the higher clamping temperatures previously assumed for the evaporator and condenser 6 (5 °C). The disadvantages of the Ocean Thermal Energy Conversion Power Plant (OTEC) are that maintenance in the deep sea is an expensive material because it is affected by corrosion from seawater. Interestingly, what could be the development of this OTEC research is the thermal energy conversion power plant on the lake.

7. Conclusions

1. The results of the development of the tin copper alloy heat exchanger model in the BJM type heat exchanger design without a hole in the middle still do not get the desired heat value, which is only a maximum of 26 °C and while the BEM type can produce an average temperature value of 30 °C, it is capable of turning the turbine, with a power output of 4.3 kW.

2. Looking at the results at each point of the 4 OTEC cycle variations on the CFD Counter Temperature BEM inlet ammonia and heating water the average result is 27.5 °C. Meanwhile, the results of the BJM Temperature Counter CFD Simulation result in an average temperature of 24.1 °C. So the variation of heat exchanger makes the BEM type the main priority in this investigation which has resulted in the expected high temperatures and pressures.

3. The simulations carried out by both Aspen Plus and Ansys CFD in the OTEC closed cycle on a new model of a copper-tin alloy heat exchanger is very effective in producing power that can rotate a turbine and produce a BEM type which will be upgraded to a prototype scheme for future researchers as a representative material from titanium that has not been reached by many people in coastal areas.

Conflict of interest

The authors declare that they have no conflict of interest in relation to this research, whether financial, personal, authorship or otherwise, that could affect the research and its results presented in this paper.

Acknowledgment

In this opportunity, the writer would like to express deep gratitude to:

1. Prof. Basuki Wirjosentono, MS, PhD, as dissertation supervisor one in this research, from the Mathematics and Natural Sciences Faculty of Universitas Sumatera Utara.

2. Prof. Dr. Eng Himsar Ambarita ST. MT as dissertation supervisor two in this research, from the Mechanical Engineering Faculty of Universitas Sumatera Utara.

3. Prof. Jaswar Koto as dissertation supervisor three in this research, Vice Rector for Academic Affairs, Research & Development and Digital Advancement of Universitas Insan Cita Indonesia.

4. Colleagues, both seniors, and students who are actively involved in this research, cannot be mentioned one by one.

References

1. Adiputra, R., Utsunomiya, T., Koto, J., Yasunaga, T., Ikegami, Y. (2019). Preliminary design of a 100 MW-net ocean thermal energy conversion (OTEC) power plant study case: Mentawai island, Indonesia. Journal of Marine Science and Technology, 25 (1), 48–68. doi: https://doi.org/10.1007/s00773-019-00630-7
2. García Huante, A., Rodríguez Cueto, Y., Hernández Contreras, R. E., Garduño Ruíz, E. P., Alatorre Mendieta, M. Á., Silva, R. (2021). Validation of Sea-Surface Temperature Data for Potential OTEC Deployment in the Mexican Pacific. Energies, 14 (7), 1898. doi: https://doi.org/10.3390/en14071898
3. Langer, J., Quist, J., Blok, K. (2021). Review of Renewable Energy Potentials in Indonesia and Their Contribution to a 100 % Renewable Electricity System. Energies, 14 (21), 7033. doi: https://doi.org/10.3390/en14217033
4. Jin, Z., Ye, H., Wang, H., Li, H., Qian, J. (2017). Thermodynamic analysis of siphon flash evaporation desalination system using ocean thermal energy. Energy Conversion and Management, 136, 66–77. doi: https://doi.org/10.1016/j.enconman.2017.01.002
5. Herrera, J., Sierra, S., Ibeas, A. (2021). Ocean Thermal Energy Conversion and Other Uses of Deep Sea Water: A Review. Journal of Marine Science and Engineering, 9 (4), 356. doi: https://doi.org/10.3390/jmse9040356
6. Hunt, J. D., Nascimento, A., Zakeri, B., Barbosa, P. S. F., Costalonga, L. (2022). Seawater air-conditioning and ammonia district cooling: A solution for warm coastal regions. Energy, 254, 124359. doi: https://doi.org/10.1016/j.energy.2022.124359
7. Kulyk, V., Teptya, V., Vishnevskyi, S., Hrytsiuk, Y., Hrytsiuk, I., Zatkhei, M. (2022). Development of a method for optimizing industrial energy storage units placement in electric distribution networks on the basis of ideal current distribution. Eastern-European Journal of Enterprise Technologies, 3 (8 (117)), 6–16. doi: https://doi.org/10.15587/1729-4061.2022.260080
8. Chen, Y., Liu, Y., Zhang, L., Yang, X. (2021). Three-Dimensional Performance Analysis of a Radial-Inflow Turbine for Ocean Thermal Energy Conversion System. Journal of Marine Science and Engineering, 9 (3), 287. doi: https://doi.org/10.3390/jmse9030287
9. Zhang, H., Liu, C., Yang, Y., Wang, S. (2020). Ocean thermal energy utilization process in underwater vehicles: Modelling, temperature boundary analysis, and sea trail. International Journal of Energy Research, 44 (4), 2966–2983. doi: https://doi.org/10.1002/er.5123
10. Hunt, J. D., Weber, N. de A. B., Zakeri, B., Diaby, A. T., Byrne, P., Filho, W. L., Schneider, P. S. (2021). Deep seawater cooling and desalination: Combining seawater air conditioning and desalination. Sustainable Cities and Society, 74, 103257. doi: https://doi.org/10.1016/j.scs.2021.103257
11. Langer, J., Infante Ferreira, C., Quist, J. (2022). Is bigger always better? Designing economically feasible ocean thermal energy conversion systems using spatiotemporal resource data. Applied Energy, 309, 118414. doi: https://doi.org/10.1016/j.apenergy.2021.118414
12. Kovalenko, V., Borysenko, A., Kotok, V., Nafeev, R., Verbitskiy, V., Melnyk, O. (2022). Determination of technological parameters of Zn-Al layered double hydroxides, as a matrix for functional anions intercalation, under different synthesis conditions. Eastern-European Journal of Enterprise Technologies, 2 (6 (116)), 25–32. doi: https://doi.org/10.15587/1729-4061.2022.254496
13. Chen, Y., Liu, Y., Yang, W., Wang, Y., Zhang, L., Wu, Y. (2021). Research on Optimization and Verification of the Number of Stator Blades of kW Ammonia Working Medium Radial Flow Turbine in Ocean Thermal Energy Conversion. Journal of Marine Science and Engineering, 9 (8), 901. doi: https://doi.org/10.3390/jmse9080901
14. Seungtaek, L., Hoseang, L., Hyeonju, K. (2020). Dynamic Simulation of System Performance Change by PID Automatic Control of Ocean Thermal Energy Conversion. Journal of Marine Science and Engineering, 8 (1), 59. doi: https://doi.org/10.3390/jmse8010059
15. Vera, D., Baccioli, A., Jurado, F., Desideri, U. (2020). Modeling and optimization of an ocean thermal energy conversion system for remote islands electrification. Renewable Energy, 162, 1399–1414. doi: https://doi.org/10.1016/j.renene.2020.07.074
16. Rapaka, V., Bakkiyanathan, M. (2013). Mathematical Modelling of A Plate Type Heat Exchanger for A 0.1 MWe OTEC Plant. International Journal of Engineering Research & Technology (IJERT), 2 (7). Available at: https://www.ijert.org/research/mathematical-modelling-of-a-plate-type-heat-exchanger-for-a-0.1-mwe-otec-plant-IJERTV2IS70570.pdf
17. Zapata, A., Amaris, C., Sagastume, A., Rodríguez, A. (2021). CFD modelling of the ammonia vapour absorption in a tubular bubble absorber with $NH_3/LiNO_3$. Case Studies in Thermal Engineering, 27, 101311. doi: https://doi.org/10.1016/j.csite.2021.101311
18. Ghavami, N., Özdenkçi, K., Chianese, S., Musmarra, D., De Blasio, C. (2022). Process simulation of hydrothermal carbonization of digestate from energetic perspectives in Aspen Plus. Energy Conversion and Management, 270, 116215. doi: https://doi.org/10.1016/j.enconman.2022.116215